Editors' Suggestion | Featured in Physics

Depletion of Two-Level Systems in Ultrastable Computer-Generated Glasses

Dmytro Khomenko,[1,2,†] Camille Scalliet,[3,†,*] Ludovic Berthier,[4,5]
David R. Reichman,[2] and Francesco Zamponi[1]

[1]*Laboratoire de Physique de l'Ecole Normale Supérieure, ENS, Université PSL, CNRS, Sorbonne Université, Université de Paris, 75005 Paris, France*
[2]*Department of Chemistry, Columbia University, New York, New York 10027, USA*
[3]*DAMTP, Centre for Mathematical Sciences, University of Cambridge, Wilberforce Road, Cambridge CB3 0WA, United Kingdom*
[4]*Department of Chemistry, University of Cambridge, Lensfield Road, Cambridge CB2 1EW, United Kingdom*
[5]*Laboratoire Charles Coulomb (L2C), Université de Montpellier, CNRS, 34095 Montpellier, France*

(Received 22 November 2019; accepted 28 April 2020; published 2 June 2020)

Amorphous solids exhibit quasiuniversal low temperature anomalies whose origin has been ascribed to localized tunneling defects. Using an advanced Monte Carlo procedure, we create *in silico* glasses spanning from hyperquenched to ultrastable glasses. Using a multidimensional path-finding protocol, we locate tunneling defects with energy splittings smaller than $k_B T_Q$, with T_Q the temperature below which quantum effects are relevant ($T_Q \approx 1$ K in most experiments). We find that as the stability of a glass increases, its energy landscape as well as the manner in which it is probed tend to deplete the density of tunneling defects, as observed in recent experiments. We explore the real-space nature of tunneling defects, and find that they are mostly localized to a few atoms, but are occasionally dramatically delocalized.

DOI: 10.1103/PhysRevLett.124.225901

The theory of low temperature properties of perfect crystals stands as one of the most profound early tests of the power of quantum statistical mechanics. In particular, Debye's calculation of the observed T^3 behavior of the low temperature specific heat highlighted the importance of long wavelength phonons as low energy excitations in ordered solids [1]. Given that the wavelength of populated phonon modes around $T \sim 1$ K is significantly longer than the interparticle distance in a solid, it came as a major surprise in 1971 when Zeller and Pohl [2] measured large deviations from the expected Debye behavior of the specific heat and the thermal conductivity of vitreous silica, selenium, and germanium-based glasses. An explanation for this puzzling observation was almost immediately put forward by Anderson, Halperin, and Varma [3], and Phillips [4]. They posited that the disorder intrinsic to amorphous solids causes their energy landscape to have many minima. Rare, nearly degenerate, adjacent local minima support tunneling defects or two-level systems (TLS) with energy splittings of the order of 1K, which provide a large excess contribution to the specific heat and a new mode of scattering that determines the thermal conductivity. In the subsequent decades, the behavior described by Zeller and Pohl was observed in numerous other amorphous materials, and the TLS theory has withstood essentially all experimental tests [5–9]. Despite this great progress, the microscopic real-space structure of the tunneling defects remains debated, as do the factors that determine their density and distribution in amorphous solids [10–22].

A powerful platform for addressing these issues is the use of computer simulation to prepare amorphous materials *in silico* and to interrogate the simulated energy landscape for TLS [23]. This program was initiated by Stillinger and Weber [24,25], then carried out more extensively by Heuer and Silbey [26–29], nearly three decades ago. Limited by the computational power and algorithms available back then, they created computer glasses with cooling rates roughly nine orders of magnitude larger than in laboratory settings. They were able to locate only a handful of TLS with the requisite tunnel splittings, necessitating uncontrolled extrapolations. The situation then improved incrementally [30–33], although the algorithmic ability to simulate glasses which are cooled in an experimentally realistic way has remained out of reach until very recently. This limited greatly our microscopic understanding of the universal anomalous thermal behavior of low temperature glasses from a computational viewpoint.

In this Letter, we leverage the remarkable ability of the swap Monte Carlo algorithm to produce *in silico* amorphous materials with fictive temperatures that range from those found in typical experiments to the significantly slower rates found in recent vapor deposition studies [34]. We find a dramatic depletion of active TLS (those with a tunnel splitting $\sim$1 K) with decreasing quench rate, as found in recent experiments [35–39], with the notable exception of old amber glasses [40]. We use a state-of-the-art reaction path-finding protocol [41,42] to efficiently locate double-well potentials in the multidimensional

potential energy landscape, yielding a *direct sampling* of tunneling states with sufficient statistics to avoid any extrapolation. We determine the degree of localization of individual TLS, providing a detailed, real-space understanding of how atoms participate in tunneling motion and how the thermal exploration of the energy landscape in well-annealed amorphous materials determines the density of tunneling centers.

Glass preparation.—Past works on the landscape of low temperature glasses focused on simple models for real materials such as NiP [26], Argon [30], and silica [32,33]. Our goal is to understand how glass preparation affects the density of TLS within a single model. We study a polydisperse mixture of particles interacting via an inverse power law potential [34]. Our choice is motivated by the fact that low temperature anomalies are observed in glasses, regardless the material. Given the diversity of models, we choose one for which swap Monte Carlo enables maximally efficient thermalization on the computer over a range of temperatures at least as wide as in experiments [34].

We provide minimal details on the system and measures of equilibration (see the Supplemental Material [43] for details). We simulate a nonadditive polydisperse mixture of $N = 1500$ particles of mass m. Two particles i and j separated by a distance r_{ij} interact via the potential

$$v(r_{ij}) = \epsilon\left(\frac{\sigma_{ij}}{r_{ij}}\right)^{12} + \epsilon F(r_{ij}/\sigma_{ij}), \tag{1}$$

only if $r_{ij} < r_{\rm cut} = 1.25\sigma_{ij}$, σ_{ij} being the nonadditive interaction length scale. The function F is a fourth-order polynomial which guarantees continuity of the potential up to the second derivative at $r_{\rm cut}$. We characterize the physical classical dynamics of the model using molecular dynamics (MD) with energies and lengths expressed in units of ϵ and the average diameter σ, respectively. Times measured during MD simulations are expressed in units of $\sqrt{\epsilon/m\sigma^2}$. Number density is set to $\rho = 1$. The relaxation time τ_α of the equilibrium fluid is measured from the self-intermediate scattering function $F_s(k = 7.0, \tau_\alpha) = e^{-1}$. The onset of glassy dynamics, signaled by deviations from Arrhenius behavior, takes place at $T_o = 0.18$, where $\tau_\alpha(T_o) \equiv \tau_o$, and the mode-coupling crossover temperature is $T_{\rm MCT} = 0.104$ [34].

We analyze *in silico* glasses by preparing fully equilibrated configurations at various preparation temperatures T_f using the swap Monte Carlo algorithm, which utilizes the exchange of particles' diameters in addition to standard translational moves, leading to a massive thermalization speed-up. Our implementation is that of Ref. [44]. The configurations are then rapidly cooled to lower temperatures using regular molecular dynamics. Therefore, T_f represents the "temperature at which the glass would find itself in equilibrium if suddenly brought to it from its given state," which is precisely the definition of Tool's fictive temperature [45]. The temperature T_f characterizes the degree of stability of the glasses, see Fig. 1(a). In experiments, T_f would be determined by the cooling rate [46,47], or the substrate temperature in a vapor deposition experiment [48–52]. We present results for glasses in wide range of stabilities: poorly annealed (hyperquenched) glasses [$T_f = 0.092$ where $\log(\tau_\alpha/\tau_o) = 4.9$, slightly below $T_{\rm MCT}$], liquid-cooled experimental glasses [$T_f = 0.07 \simeq T_g$, where $\log(\tau_\alpha/\tau_o) = 10.7$], and ultrastable glasses [$T_f = 0.062$, where $\log(\tau_\alpha/\tau_o) = 14.8$]. To obtain statistically significant results, we analyze N_g independent samples ($N_g = 200$, 50, 15 for increasing T_f).

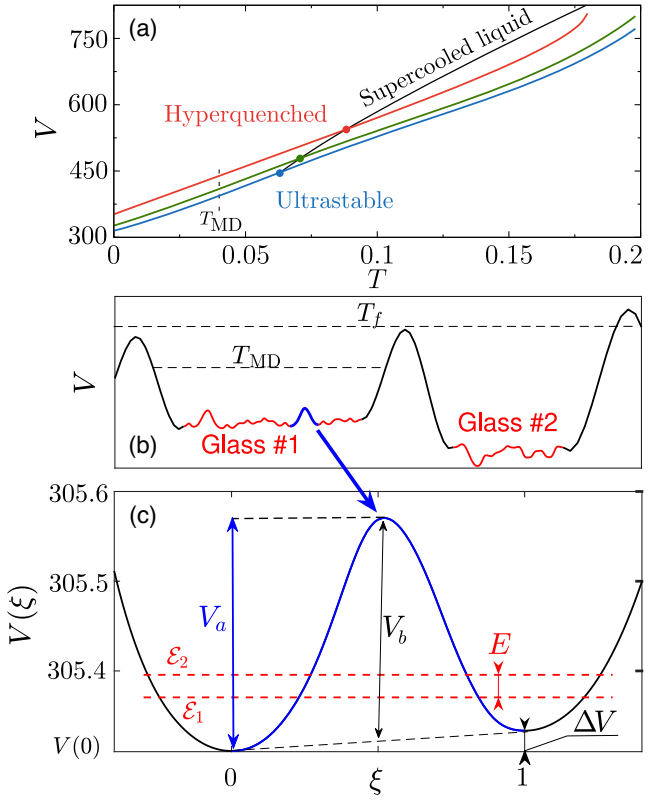

FIG. 1. (a) Glasses are prepared at equilibrium (black line) at temperatures $T_f = 0.092$, 0.07, 0.062 (bullets), from hyperquenched to ultrastable. We follow their potential energy after rapid quenches (colored lines). (b) Sketch of the potential energy landscape. Double-well potentials are detected with molecular dynamics simulations at $T_{\rm MD} = 0.04$ (blue). (c) A detected double-well potential $V(\xi)$. The classical asymmetry ΔV, activation energy V_a, energy barrier $V_b = V_a - \Delta V/2$, the energy levels, $\mathcal{E}_1$ and $\mathcal{E}_2$, of the ground-state doublet, and the tunnel splitting, $E = \mathcal{E}_2 - \mathcal{E}_1$, are illustrated.

Landscape exploration.—We identify transitions between nearby minima, or double-well potentials (DWPs) in the glasses. Briefly, starting from the configurations equilibrated at T_f, we run MD simulations at $T_{\rm MD} = 0.04$, which is sufficiently low to confine each glass in a single metabasin, but high enough that the system

can rapidly visit distinct minima (inherent structures) within the metabasin [23], see Fig. 1(b). Details are given in the Supplemental Material [43].

By sampling the inherent structures along MD trajectories [30], we obtain a library of visited minima, as well as the pairs of them that are dynamically connected. We use the isoconfigurational ensemble [53]: for each of the N_g independent configurations, we run up to 200 MD simulations, each initialized with different velocities. The number and duration of isoconfigurational runs is large enough for the probability distribution function (pdf) of the inherent structures potential energy, and the number of transitions, to reach stationarity. While we reach convergence of the pdfs, all possible minima are not sampled, and their numbers increase with additional runs. We however sample a significant number of minima: 13 252, 26 898, 848 698 for $T_f = 0.062$, 0.07, 0.092, respectively. As shown below, this is enough to directly determine the density of tunneling TLS.

We select transitions between adjacent minima as described in the Supplemental Material [43]. We compute the minimum energy path connecting each pair of minima using a climbing image nudged elastic band (NEB) algorithm [41,42], which ensures the accurate determination of the saddle point, and provides a smooth energy profile. Occasionally, especially for $T_f = 0.092$, the NEB energy profile contains intermediate minima. In such cases, we apply an iterative method to split the energy profile into distinct DWPs, which are then analyzed similarly to the other ones.

We parametrize a DWP by its potential energy $V(\xi)$ along the minimum energy path, with $\xi = 0$, 1 corresponding to the two minima (we arbitrarily choose $\xi = 0$ for the deepest minimum), see Fig. 1(c). A DWP is characterized by its asymmetry $\Delta V = V(1) - V(0)$, energy barrier $V_b = V_a - \Delta V/2$, where V_a is the activation energy, and the distance d between minima. The distance is calculated along the reaction coordinate given by the NEB, as the sum of Euclidean distances between images of the system: $d^2 = \sum_{i,\mu} d_{i,\mu}^2$, where $d_{i,\mu}$ is the displacement of particle i in direction $\mu = x$, y, z. The participation ratio, $\mathrm{PR} = d^4/(\sum_{i,\mu} d_{i,\mu}^4)$, characterizes the number of particles involved in the transition.

We present in Fig. 2 the statistics of the DWP parameters. The pdfs for $T_f = 0.062$ and 0.07 agree quantitatively, within noise, while we observe an evolution for $T_f = 0.092$. In particular, the pdfs of asymmetries and energy barriers are almost exponential in all glasses. The mild dependence of these tails on T_f may stem from the fact that the sampling temperature T_{MD} sets a limit on the DWPs that can be detected, independently of T_f (see the Supplemental Material [43] for the effect of T_{MD}). While the distribution of energy asymmetry is exponential at high energies ΔV, it becomes flat at low energies where

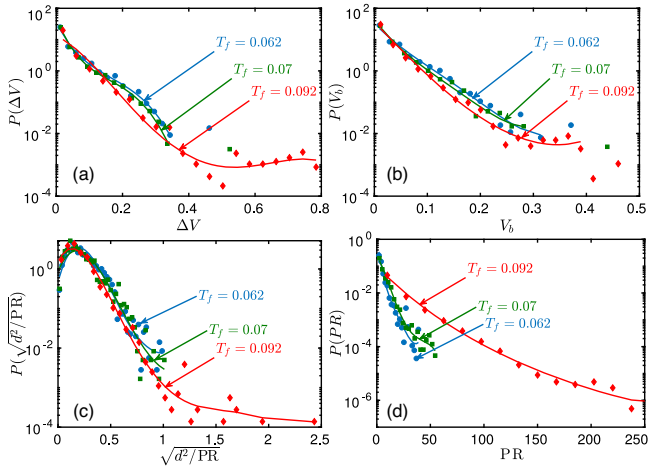

FIG. 2. Probability distribution functions of DWP parameters as a function of glass preparation temperature T_f: (a) asymmetry ΔV, (b) energy barrier V_b, (c) distance d normalized by $\sqrt{\mathrm{PR}}$, which characterizes the typical individual displacement of particles that participate actively in a double-well transition, and (d) participation ratio (PR). Lines are a guide for the eye.

TLS are found (see Fig. S6). The pdfs of distances (not shown) and participation ratios vary more significantly between $T_f \leq 0.07$ and $T_f = 0.092$. Since $d \propto \sqrt{\mathrm{PR}}$, an increase of PR will affect the distribution of d. We instead study the pdf of $d/\sqrt{\mathrm{PR}}$. This quantity can be interpreted as an average displacement of the particles that participate in the transition. On average, the number of particles involved in DWPs is larger in poorly annealed glasses, while the displacements of individual particles remain comparable. To our knowledge, the dependence of the quench rate on DWPs classical parameters has not yet been reported. Note that TLS typically correspond to DWPs with very small ΔV and relatively large V_b. The tunnel splitting stems from nontrivial correlations between the classical parameters [30], thus the pdfs of classical parameters alone are not informative on quantum tunneling (see the Supplemental Material [43]).

Density of two-level systems.—At sufficiently low temperatures, thermal activation over the energy barrier V_b is suppressed, and quantum tunneling becomes important [54]. In our analysis, we reduce the problem to a one dimensional effective Schrödinger equation along the reaction coordinate. Following Vineyard [55], the effective mass remains m, with a reaction coordinate $x \in [0, d]$. Using the normalized variable $\xi = x/d$, and scaling energies by ϵ, we obtain

$$-\frac{\hbar^2}{2md^2\epsilon}\partial_\xi^2\Psi(\xi) + V(\xi)\Psi(\xi) = \mathcal{E}\Psi(\xi), \tag{2}$$

where the "quantumness" of the problem is controlled by the dimensionless mass $\tilde{m} = m\sigma^2\epsilon/\hbar^2$ (see Fig. 3). In general, the Laplacian should take into account curvature

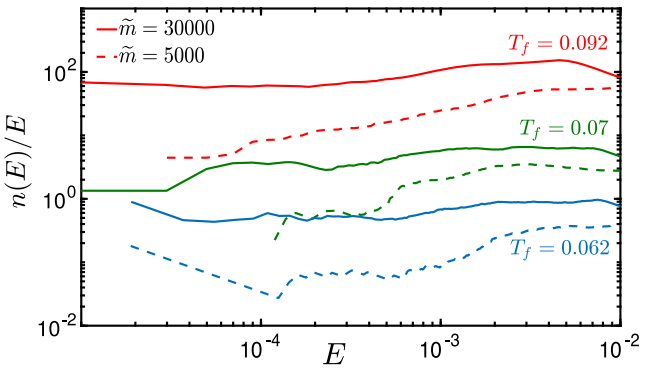

FIG. 3. Cumulative distribution of energy splitting $n(E)$ divided by E, from hyperquenched to ultrastable glasses (top to bottom). The values $\tilde{m}$ are chosen for comparison with real materials. The plateau at small E affords a direct determination of the TLS density n_0, which is suppressed by two orders of magnitude as glass preparation is varied.

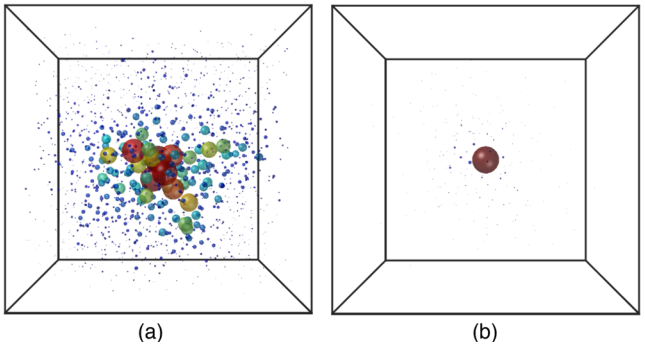

FIG. 4. Snapshots of TLS with low tunnel splitting E for $T_f = 0.092$ and $\tilde{m} = 30000$. (a) PR ≈ 126 with $E = 8.9 \times 10^{-5}$. (b) PR ≈ 1.6 and similarly low $E = 5.4 \times 10^{-5}$. The size and color of particles are proportional to their displacement between the initial and final configurations of the TLS, normalized to the highest displacement.

effects, which we neglect here.The potential $V(\xi)$ obtained from the NEB is defined in $\xi \in [0, 1]$. To solve Eq. (2), we extrapolate it outside this interval (see the Supplemental Material [43]).

We solve Eq. (2) for all DWPs. We compute the first two energy levels, $\mathcal{E}_1$ and $\mathcal{E}_2$, of the double well and define the tunnel splitting $E = \mathcal{E}_2 - \mathcal{E}_1$. We illustrate in Fig. 1(c) the two energy levels and tunnel splitting of a DWP. The tunnel splitting E is the relevant parameter for low temperature properties. The transitions that occur by quantum tunneling have a tunnel splitting $E \sim T$ [6]. These particular DWPs are called tunneling two-level systems (TLS).

We characterize the distribution of TLS using a cumulative distribution of tunnel splittings $n(E)$, defined as the number of DWPs with tunnel splitting smaller than E, normalized by the number of particles N in the glass, and the number of independent samples N_g. In TLS theory, $n(E)$ can be expanded as $n(E) \simeq n_0 E + \mathcal{O}(E^2)$ for small E, the specific heat at low temperature is linear with T, and n_0 enters the prefactor [3,6].

In order to estimate the density n_0 of TLS and its dependence on glass stability, we plot $n(E)/E$ as a function of tunnel splitting E in Fig. 3. All curves indicate a saturation to a plateau value, n_0, at low E. The existence of a plateau value demonstrates our ability to directly estimate the density of TLS n_0 without any uncontrolled extrapolation. Data on tunneling rates [56] and distribution of tunneling matrix elements Δ_0 are presented in the Supplemental Material [43].

Our key result is that the TLS density n_0 [as estimated by $n(E)/E$ in the range 10^{-3}–10^{-4}] decreases by two orders of magnitude from hyperquenched to ultrastable glasses. To our knowledge, this constitutes the first numerical evidence for a significant suppression of TLS with increasing glass stability.

Microscopic nature of TLS.—How many particles are involved in the tunneling motion of a TLS [30–33]? We analyzed how the participation ratio of transitions correlates with the tunnel splitting E. We find that the participation ratio of low temperature active TLS with tunnel splittings $E \sim 10^{-3}$–10^{-4} varies from 1 to 200 (see the Supplemental Material [43]). The higher participation ratios (PR ~ 200) are found in hyperquenched glasses, while in ultrastable glasses the participation ratio rarely exceeds $\sim$30. We provide systematic numerical evidence that TLS active at low temperature are typically very localized, but occasionally associated with collective excitations. We provide two snapshots in Fig. 4, corresponding to a collective TLS (left) and a very localized TLS (right) identified in a hyperquenched glass.

Discussion.—Our study of tunneling TLS in a simple computer model demonstrates their importance to understand low temperature glass anomalies. We show that the density n_0 of TLS directly controls the linear temperature dependence of the specific heat at low temperatures. Several recent works advocated the idea that quantized low-frequency harmonic modes alone could explain this behavior [10,18,57–61]. These soft modes are known for our glasses [62], but we find that their contribution to the low temperature specific heat is subdominant (see the Supplemental Material [43]), suggesting that the specific heat of structural glasses is dominated by tunneling TLS, as originally proposed in [3,6].

To relate our data to experiments we convert simulation units into physical ones. The temperature scale below which quantum effects become important is obtained by comparing the thermal wavelength to the interparticle distance: $T_Q = (2\pi\hbar^2)/(m\sigma^2 k_B)$. We consider DWPs with $E < k_B T_Q$ as low temperature active TLS, and their total number is $n_{\text{active}} = N N_g n(E = k_B T_Q)$.

A detailed analysis on experimental comparisons is presented in the Supplemental Material [43]. We first

consider Argon parameters: $\sigma = 3.4 \times 10^{-10}$ m, $\epsilon/4 = 1.65 \times 10^{-21}$ J, $m = 6 \times 10^{-26}$ kg [30]. This gives $T_g \sim 32$ K, $T_Q \sim 0.73$ K, and $\tilde{m} \sim 4000$. For this choice, we estimate from Fig. 3 $n_0^{\mathrm{sim}} \sim 4$, 0.4, 0.04 for increasing glass stability. This gives $n_0^{\mathrm{exp}} \sim 10^{49}, 10^{48}, 10^{47}$ J^{-1} m^{-3}. Active TLS have $E < k_B T_Q = 0.0015\epsilon$ and we find $n_{\mathrm{active}} = 1008$, 291, 61 such TLS for $T_g = 0.092$, 0.07, 0.062, respectively. A second choice motivated by NiP metallic glasses [26] would be to use Nickel as a reference, for which $\sigma = 2.21 \times 10^{-10}$ m, $\epsilon = 6.14 \times 10^{-20}$ J, $m = 1.02 \times 10^{-25}$ kg [63]. In this case, we have $T_g \sim 298$ K, $T_Q \sim 0.9$ K, and $\tilde{m} \sim 30000$. For this value of $\tilde{m}$, we find $n_0^{\mathrm{sim}} \sim 60$, 6, 0.6 for $T_f = 0.092$, 0.07, 0.062, yielding $n_0^{\mathrm{exp}} \sim 10^{50}, 10^{49}, 10^{48}$ J^{-1} m^{-3}. Active TLS have $E < k_B T_Q = 0.0002\epsilon$ and we find $n_{\mathrm{active}} = 248$, 46, 28 such TLS for $T_g = 0.092$, 0.07, 0.062, respectively.

Experimentally, a value of $n_0 \sim 10^{46}$ J^{-1} m^{-3} is reported [6,7]. Our estimation for $T_f = 0.07$ is larger by a factor $\sim 10^2$–10^3 (Argon and Nickel, respectively). It is difficult to rationalize this discrepancy but we can offer several hypothesis. One possibility is that we include in our estimates all DWPs detected at temperature $T_{\mathrm{MD}} = 0.04 \gg T_Q$, while, experimentally, the glass is directly brought to T_Q and only a small fraction of TLS that lie at the bottom of the energy metabasin would be excited. Furthermore, not all TLS would tunnel on the relevant timescales: it is known that $n_0 \sim \log(\tau)$ where τ is the observation time at T_Q [6]. This should persist up to the timescale of complete exploration of the energy landscape. Our exploration protocol at $T_{\mathrm{MD}} \gg T_Q$ artificially sets τ larger than this cutoff (see the Supplemental Material [43] for the tunneling rates of TLS). Another explanation could be that our model is too simple to describe real molecular materials, for example network glasses. Since we analyze a single model, the fundamental question of universality in TLS density remains unanswered. Analyzing different glass-forming models will be crucial to answer this question.

The reduction of n_0 by two orders of magnitude when moving from hyperquenched to ultrastable glasses is robust and in good agreement with recent experiments [36,39]. We show that for a given glass-forming model, glass preparation affects dramatically the density of TLS. Our results demonstrate that glass ultrastability (rather than potential anisotropy of the vapor-deposited samples) is responsible for the depletion of TLS.

We thank M. Ediger, D. Rodney and W. Ji for discussions. This project received funding from the European Research Council (ERC) under the European Union's Horizon 2020 research and innovation program (Grant No. 723955—GlassUniversality, and Grant No. 740269—ADNeSP), and from the Simons Foundation (Grant No. 454933, L. B., Grant No. 454955, F. Z., Grant No. 454951 D. R.). C. S. acknowledges the Fondation l'Oréal.

*cs2057@cam.ac.uk
†These authors contributed equally to this work.

[1] N. W. Ashcroft and N. D. Mermin, *Solid State Physics* (Thomson Learning, New York, 1976).
[2] R. C. Zeller and R. O. Pohl, Phys. Rev. B **4**, 2029 (1971).
[3] P. W. Anderson, B. I. Halperin, and C. M. Varma, Philos. Mag. **25**, 1 (1972).
[4] W. Phillips, J. Low Temp. Phys. **7**, 351 (1972).
[5] M. T. Loponen, R. C. Dynes, V. Narayanamurti, and J. P. Garno, Phys. Rev. B **25**, 1161 (1982).
[6] W. A. Phillips, Rep. Prog. Phys. **50**, 1657 (1987).
[7] J. F. Berret and M. Meißner, Z. Phys. B **70**, 65 (1988).
[8] A.-M. Boiron, P. Tamarat, B. Lounis, R. Brown, and M. Orrit, Chem. Phys. **247**, 119 (1999).
[9] A. L. Burin, J. M. Leveritt III, G. Ruyters, C. Schötz, M. Bazrafshan, P. Fassl, M. von Schickfus, A. Fleischmann, and C. Enss, Europhys. Lett. **104**, 57006 (2013).
[10] Y. M. Galperin, V. Karpov, and V. Kozub, Adv. Phys. **38**, 669 (1989).
[11] S. N. Coppersmith, Phys. Rev. Lett. **67**, 2315 (1991).
[12] A. J. Leggett, Physica (Amsterdam) **169B**, 322 (1991).
[13] A. Burin and Y. Kagan, Phys. Lett. A **215**, 191 (1996).
[14] D. R. Reichman, P. Neu, and R. J. Silbey, Mol. Cryst. Liq. Cryst. Sci. Technol., Sect. A **291**, 65 (1996).
[15] V. Lubchenko and P. G. Wolynes, Phys. Rev. Lett. **87**, 195901 (2001).
[16] V. Gurarie and J. T. Chalker, Phys. Rev. B **68**, 134207 (2003).
[17] V. Lubchenko and P. G. Wolynes, Proc. Natl. Acad. Sci. U.S.A. **100**, 1515 (2003).
[18] D. A. Parshin, H. R. Schober, and V. L. Gurevich, Phys. Rev. B **76**, 064206 (2007).
[19] D. C. Vural and A. J. Leggett, J. Non-Cryst. Solids **357**, 3528 (2011).
[20] A. J. Leggett and D. C. Vural, J. Phys. Chem. B **117**, 12966 (2013).
[21] D. Zhou and A. J. Leggett, arXiv:1510.05538.
[22] H. M. Carruzzo and C. C. Yu, Phys. Rev. Lett. **124**, 075902 (2020).
[23] A. Heuer, J. Phys. Condens. Matter **20**, 373101 (2008).
[24] F. H. Stillinger and T. A. Weber, Phys. Rev. A **25**, 978 (1982).
[25] T. A. Weber and F. H. Stillinger, Phys. Rev. B **32**, 5402 (1985).
[26] A. Heuer and R. J. Silbey, Phys. Rev. Lett. **70**, 3911 (1993).
[27] A. Heuer and R. J. Silbey, Phys. Rev. B **49**, 1441 (1994).
[28] D. Dab, A. Heuer, and R. Silbey, J. Lumin. **64**, 95 (1995).
[29] A. Heuer and R. J. Silbey, Phys. Rev. B **53**, 609 (1996).
[30] F. Demichelis, G. Viliani, and G. Ruocco, PhysChemComm **2**, 20 (1999).
[31] J. Reinisch and A. Heuer, Phys. Rev. B **70**, 064201 (2004).
[32] J. Reinisch and A. Heuer, Phys. Rev. Lett. **95**, 155502 (2005).
[33] T. Damart and D. Rodney, Phys. Rev. B **97**, 014201 (2018).
[34] A. Ninarello, L. Berthier, and D. Coslovich, Phys. Rev. X **7**, 021039 (2017).

[35] D. R. Queen, X. Liu, J. Karel, T. H. Metcalf, and F. Hellman, Phys. Rev. Lett. **110**, 135901 (2013).
[36] T. Pérez-Castañeda, C. Rodríguez-Tinoco, J. Rodríguez-Viejo, and M. A. Ramos, Proc. Natl. Acad. Sci. U.S.A. **111**, 11275 (2014).
[37] X. Liu, D. R. Queen, T. H. Metcalf, J. E. Karel, and F. Hellman, Phys. Rev. Lett. **113**, 025503 (2014).
[38] M. D. Ediger, Proc. Natl. Acad. Sci. U.S.A. **111**, 11232 (2014).
[39] D. R. Queen, X. Liu, J. Karel, H. C. Jacks, T. H. Metcalf, and F. Hellman, J. Non-Cryst. Solids **426**, 19 (2015).
[40] T. Pérez-Castañeda, R. J. Jiménez-Riobóo, and M. A. Ramos, Phys. Rev. Lett. **112**, 165901 (2014).
[41] H. Jónsson, G. Mills, and K. W. Jacobsen, in *Classical and Quantum Dynamics in Condensed Phase Simulations*, edited by B. J. Berne, G. Ciccotti, and D. F. Coker (World Scientific, Singapore, 1998).
[42] G. Henkelman, B. P. Uberuaga, and H. Jónsson, J. Chem. Phys. **113**, 9901 (2000).
[43] See the Supplemental Material at http://link.aps.org/supplemental/10.1103/PhysRevLett.124.225901 for details on the numerical exploration of the landscape, quantum splitting computation, numerical tests of the TLS theory, and the TLS contribution to the specific heat.
[44] L. Berthier, E. Flenner, C. J. Fullerton, C. Scalliet, and M. Singh, J. Stat. Mech. (2019) 064004.
[45] A. Q. Tool, J. Am. Ceram. Soc. **29**, 240 (1946).
[46] M. D. Ediger, C. A. Angell, and S. R. Nagel, J. Phys. Chem. **100**, 13200 (1996).
[47] A. Cavagna, Phys. Rep. **476**, 51 (2009).
[48] S. F. Swallen, K. L. Kearns, M. K. Mapes, Y. S. Kim, R. J. McMahon, M. D. Ediger, T. Wu, L. Yu, and S. Satija, Science **315**, 353 (2007).
[49] K. L. Kearns, S. F. Swallen, M. D. Ediger, T. Wu, Y. Sun, and L. Yu, J. Phys. Chem. B **112**, 4934 (2008).
[50] M. Tylinski, Y. Chua, M. Beasley, C. Schick, and M. Ediger, J. Chem. Phys. **145**, 174506 (2016).
[51] M. D. Ediger, J. Chem. Phys. **147**, 210901 (2017).
[52] J. Ràfols-Ribé, M. Gonzalez-Silveira, C. Rodríguez-Tinoco, and J. Rodríguez-Viejo, Phys. Chem. Chem. Phys. **19**, 11089 (2017).
[53] A. Widmer-Cooper, P. Harrowell, and H. Fynewever, Phys. Rev. Lett. **93**, 135701 (2004).
[54] M. J. Gillan, J. Phys. C **20**, 3621 (1987).
[55] G. H. Vineyard, J. Phys. Chem. Solids **3**, 121 (1957).
[56] A. Andreassen, D. Farhi, W. Frost, and M. D. Schwartz, Phys. Rev. D **95**, 085011 (2017).
[57] L. Gil, M. A. Ramos, A. Bringer, and U. Buchenau, Phys. Rev. Lett. **70**, 182 (1993).
[58] D. A. Parshin, Phys. Rev. B **49**, 9400 (1994).
[59] W. Ji, M. Popović, T. W. J. de Geus, E. Lerner, and M. Wyart, Phys. Rev. E **99**, 023003 (2019).
[60] S. Franz, T. Maimbourg, G. Parisi, and A. Scardicchio, Proc. Natl. Acad. Sci. U.S.A. **116**, 13768 (2019).
[61] M. Baggioli, R. Milkus, and A. Zaccone, Phys. Rev. E **100**, 062131 (2019).
[62] L. Wang, A. Ninarello, P. Guan, L. Berthier, G. Szamel, and E. Flenner, Nat. Commun. **10**, 26 (2019).
[63] W. Ching and C. C. Lin, in *Amorphous Magnetism II* (Springer, New York, 1977), pp. 469–477.